Chaos, Solitons and Fractals 162 (2022) 112530

Contents lists available at ScienceDirect

Chaos, Solitons and Fractals

journal homepage: www.elsevier.com/locate/chaos

Numerical search for the stationary quasi-breather of the graphene superlattice equation

Francisca Martin-Vergara [*,1], Francisco Rus[1], Francisco R. Villatoro[1]

Escuela de Ingenierías Industriales, Dept. de Lenguajes y Ciencias de la Computación, Universidad de Málaga, 29071 Málaga, Spain

ARTICLE INFO

Keywords:
Nonlinear electromagnetic waves
Solitons
Computational simulations
Modified sine-Gordon equation
Finite difference method

ABSTRACT

The propagation of electromagnetic solitons in a graphene superlattice device is governed by a modified sine-Gordon equation, referred to as the graphene superlattice equation. Kink-antikink collisions suggest the existence of a quasi-breather solution. Here, a numerical search for static quasi-breathers is undertaken by using a new initial condition obtained by a regular perturbation of the null solution. Our results show that the frequency of the initial condition has a minimum critical value for the appearance of a robust quasi-breather able to survive during more than one thousand periods. The amplitude and energy of the quasi-breather solution decrease, but its frequency increases, as time grows. The robustness of the new quasi-breather supports its experimental search in real graphene superlattice devices.

1. Introduction

The graphene superlattice (GSL) equation [1] governs the propagation of electromagnetic waves in the planar graphene superlattice proposed by Ratnikov [2]. A comprehensive derivation of the GSL equation, a modified sine-Gordon (sG) equation, is reviewed in Ref. [3]. Ratnikov's superlattice can be fabricated by depositing a graphene sheet on a substrate with alternating layers of two materials, one that introduces a gap into the electronic structure of the graphene and another one that does not [4]; although there are alternative fabrication techniques [5,6].

The GSL equation has topological solitons (kinks and antikinks) which are not true solitons since it is non-integrable [7]. Hence, this equation does not have multi-soliton solutions, like breathers, as have integrable equations [8]. The interactions between kinks and antikinks of the Klein–Gordon equation with different nonlinearities have been widely studied in the literature [9–17]. For the GSL equation, these authors have recently studied the inelastic collision of kinks and antikinks with the same but opposite speed by using numerical methods [18]. Both solitons escape to infinity when their common initial speed is either larger than a critical value or inside some resonance windows within a fractal structure; otherwise, they form breather-like states that slowly decay by radiating energy. These breather-like states also referred to as quasi-breathers [19–21], pulsons [22], or oscillons [23,24], are long-lived localized solutions that slowly lose energy; the longevity of these solutions during thousands of oscillatory periods makes them appealing for real applications.

The numerical search for quasi-breather solutions in Klein–Gordon equations, like the GSL equation, requires the use of a good approximation to the exact solution as initial condition. For small amplitude quasi-breathers, the GSL equation can be approximated by a nonlinear Schrödinger equation with an exact breather solution, which is the preferred initial condition for the numerical search [25]; although there are alternative approaches to obtain an approximation breather solution [26]. For large amplitude quasi-breathers, an asymptotic expansion of the solution based on the breather of the sG equation as an ansatz is the most widely used initial condition [27,28]; usually, this asymptotic approximation corresponds to the maximum amplitude of the oscillatory profile of the quasi-breather at the initial time. The main drawback of the latter approach is that the asymptotic expansion is singular, requiring a multiple-scale perturbation analysis.

In this paper, an alternative initial condition for the numerical search of the quasi-breather is introduced, specifically, an asymptotic approximation to the null amplitude of its oscillatory profile. The main advantage of this approach is that the corresponding asymptotic expansion is regular, resulting in an accurate initial condition easy to obtain without using a multiple-scale perturbation analysis. Another novelty of this paper is that the GSL equation is a modification of the sG equation with a nonlinearity that shares more features with it than other Klein–Gordon equations, like the double-sine Gordon equation or the ϕ^4 model. In particular, the nonlinearities of the GSL and sG equations share the same period, having only one maximum and one

* Corresponding author.
E-mail addresses: fmarver@uma.es (F. Martin-Vergara), fdrus@uma.es (F. Rus), frvillatoro@uma.es (F.R. Villatoro).
[1] All authors have contributed equally to every stage of this article.

https://doi.org/10.1016/j.chaos.2022.112530
Received 17 March 2022; Received in revised form 22 July 2022; Accepted 2 August 2022
Available online 11 August 2022

minimum inside each period, reaching both extremes with the same absolute amplitude. These properties suggest that a good quasi-breather solution similar to the breather of the sG equation is expected for the GSL equation.

The main goal of this paper is the numerical search for a breather-like, oscillating mode in the graphene superlattice equation. Its contents are as follows. In Section 2, we present the graphene superlattice equation. In Section 2.1, we introduce and analyse the numerical scheme used to solve the equation. The initial condition used for the search of the quasi-breather is presented in Section 2.2. Our main results are presented in Section 3, including a characterization of the quasi-breathers of the GSL equation. In Section 3.1, the different solutions obtained as the frequency of the initial condition increases are characterized. In Section 3.2, the evolution in time of the parameters of the quasi-breather solutions is presented. And in Section 3.3 the long-time stability of the quasi-breather is analysed. Finally, in Section 4, some conclusions and future research lines are drawn.

2. Graphene superlattice equation

Nonlinear electromagnetic waves can propagate in a planar graphene superlattice subjected to irradiation with a frequency much larger than the plasma frequency. Their propagation along the graphene superlattice axis is governed by a nonlinear d'Alembert equation for the amplitude of the transversal component of the vector potential of the electromagnetic wave field, α, solving the nonlinear Klein–Gordon equation given by [1,3]

$$\frac{\partial^2\alpha}{\partial t^2} - c^2\,\frac{\partial^2\alpha}{\partial x^2} + \frac{\omega_{pl}^2\, b^2\, \sin\alpha}{\sqrt{1+b^2\,(1-\cos\alpha)}} = 0, \tag{1}$$

where b is a geometrical parameter associated to the superlattice, and ω_{pl} is the plasma frequency.

With the change of variables $t' = \omega_{pl}\, b\, t$, $x' = \omega_{pl}\, b\, x/c$, and $u = \alpha$, Eq. (1) results in the graphene superlattice equation, given by

$$\frac{\partial^2 u}{\partial t^2} - \frac{\partial^2 u}{\partial x^2} + \frac{dG(u)}{du} = 0, \tag{2}$$

with

$$\frac{dG(u)}{du} = \frac{\sin u}{\sqrt{1+b^2\,(1-\cos u)}},$$

where the primes have been dropped and

$$G(u) = \frac{2\,(1-\cos u)}{1+\sqrt{1+b^2\,(1-\cos u)}}. \tag{3}$$

Note that for $b = 0$, i.e., $G(u) = 1-\cos u$, the sG equation is obtained. A solitary wave solution of Eq. (2) with speed v is found by Lorentz boosting a stationary solution $u(x)$, i.e., $u(x,t) = u((x - v\,t)/\sqrt{1-v^2})$, that solves

$$\frac{d^2u}{dx^2} = \frac{dG(u)}{du}, \qquad \frac{1}{2}\left(\frac{du}{dx}\right)^2 = G(u). \tag{4}$$

The solution of Eq. (4) can be obtained in implicit form, by using elliptic integrals. The resulting expression is cumbersome, so, in practice, its numerical evaluation is preferred. Note that the breather solution of the sG equation is obtained by the method of separation of variables; however, the GSL equation is not separable, hence it does not have true breather solutions.

2.1. Numerical scheme

The GSL equation (2) is a modified sine-Gordon equation. It can be solved by using a numerical scheme for the sG equation, like the Padé methods developed by the authors in Refs. [29,30]. Let us take a method inspired in the energy conservation scheme by Guo Ben-Yu et al. [31] using the same second-order stencil in time and the Strauss–Vázquez [32] treatment for the nonlinear term, but with a fourth-order central difference formula in space; this method is given by

$$\frac{U_m^{n+1} - 2\,U_m^n + U_m^{n-1}}{\Delta t^2} - \mathcal{A}(\mathrm{E})\,\frac{(U_m^{n+1} + U_m^{n-1})}{2} + H(U_m^{n+1}) = 0, \tag{5}$$

with

$$\mathcal{A}(\mathrm{E}) = \frac{-\mathrm{E}^{-2} + 16\,\mathrm{E}^{-1} - 30 + 16\,\mathrm{E}^{1} - \mathrm{E}^{2}}{12\,\Delta x^2},$$

and

$$H(U_m^{n+1}) \equiv \frac{G(U_m^{n+1}) - G(U_m^{n-1})}{U_m^{n+1} - U_m^{n-1}},$$

where $U_m^n \approx u(x_m,t^n) = u_m^n$, $x_m = m\,\Delta x$, for $m \in \mathbb{Z}$, Δx is the grid size, $t^n = n\,\Delta t$, for $n \in \mathbb{N}$, Δt is the time step, $\mathcal{A}(\mathrm{E})\,u_m^n$ is a fourth-order discretization of the spatial derivative, and E is the shift operator defined as $\mathrm{E}\,U_m^n = U_{m+1}^n$. We use periodic boundary conditions in the finite interval $x \in (-L, L]$, with $x_m = -L + m\,\Delta x$, $m = 1, 2, \ldots, M$, and $\Delta x = 2\,L/M$ (note that $u(x_0,t) \equiv u(x_M,t)$), and a finite time interval $t \in [0,T]$, with $t^n = n\,\Delta t$, $n = 0, 1, \ldots, N$, and $\Delta t = T/N$.

Method (5) applied to the sG equation has been studied in detail by these authors in Ref. [30]. For completeness of the presentation, let us summarize its main properties for the GSL equation. First, the existence, uniqueness, and regularity of the solutions of the initial–boundary value problem for the nonlinear Klein–Gordon equation with bounded nonlinearity is known from the literature [33]: for a regular enough initial condition, the classical solution achieves the same regularity, and there is no problem with the consistency in both space and time for the numerical method. Hence, the initial-value problem of the GSL equation is well-posed and the Lax–Richtmyer theorem applies: if the numerical method is consistent and (linearly) stable it will be convergent.

The consistency of Method (5) can be studied by determining its local truncation error. It can be easily calculated by the substitution of U_m^n in Method (5) with the exact solution $u(x_m,t^n)$ of Eq. (2) and expanding the result in a power series; the result is

$$\begin{aligned}\text{Eq. (2)} \; &+ \frac{\Delta x^4}{90}\,u_{xxxxxx} + \frac{\Delta t^2}{12}\,u_{xxxx} - \frac{\Delta t^2}{2}\,u_{xxtt} \\ &+ \frac{\Delta t^2}{6}\,G_{uuu}(u)\,u_t^2 + \frac{\Delta t^2}{2}\,G_{uu}(u)\,u_{tt} + \text{h.o.t.}\end{aligned}$$

where h.o.t. means higher-order terms, and

$$G_{uu}(u) = \frac{4\,\left(1+b^2\right)\,\cos(u) - b^2\,(3+\cos(2\,u))}{4\,\left(1+b^2\,(1-\cos(u))\right)^{3/2}},$$

$$G_{uuu}(u) = \frac{\sin(u)\left(4\,(b^4+b^2)\,\cos(u) - b^4\,(\cos(2u)+3) - 16\,b^2 - 8\right)}{8\,\left(1+(b^2(1-\cos(u))\right)^{5/2}}.$$

Note that $|G_u(u)| \le 1$, $|G_{uu}(u)| \le 1$, and $|G_{uuu}(u)| \le 1$, for $b \ge 0$, so the local truncation error is bounded for a regular enough solution of the GSL equation. Hence, Method (5) is consistent with second-order in time and fourth-order in space.

The linear stability of Method (5) can be easily studied using the von Neumann analysis. The computational error $Z_m^n = U_m^n - U_m^{n*}$, with respect to a reference solution U_m^{n*} can be Fourier expanded as $Z_m^n = e^{\mathrm{i}\,m\,\beta\,\Delta x}\,\xi^n$, where $\mathrm{i} = \sqrt{-1}$, β is the spatial frequency, and ξ is the amplification factor. The condition for stability is that $|\xi| \le 1$. By introducing Z_m^n into the linearization of Method (5) and cancelling common factors, the resulting equation for ξ is given by

$$p(\xi) = A\,\xi^2 - 2\,B\,\xi + A = 0, \tag{6}$$

with

$$A = 1 + \frac{8}{3}\,r^2\,\sin^2(\omega) - \frac{1}{6}\,r^2\,\sin^2(2\,\omega), \qquad B = 1,$$

where $r = \Delta t/\Delta x$, and $\omega = \beta\,\Delta x/2$. The two roots ξ_1 and ξ_2 of the stability polynomial $p(\xi)$ have modulus smaller than or equal to unity

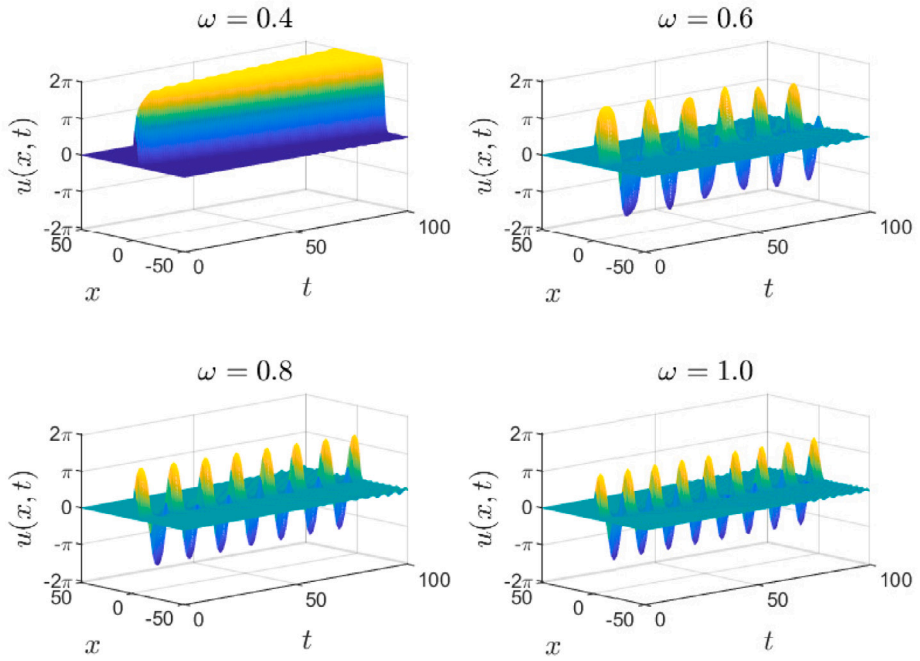

Fig. 1. Three-dimensional mesh plot of the numerical solution of the GSL equation with $b = 1$ for the initial condition (14) with $\omega = 0.4$ (top left plot), 0.6 (top right plot), 0.8 (bottom left plot), and 1.0 (bottom right plot), by using $\Delta t = \Delta x = 0.01$, $x \in [-50, 50)$, and $t \in [0, 100]$.

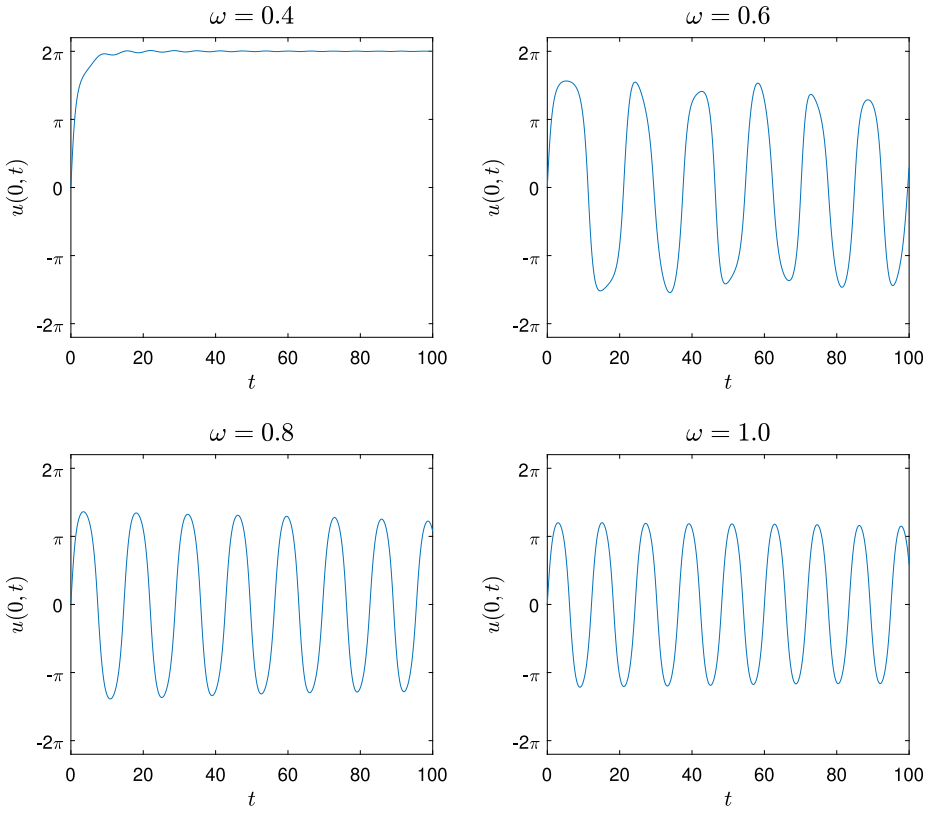

Fig. 2. The centre $u(0, t)$ of the numerical solutions of the GSL equation with $b = 1$ shown in Fig. 1.

for every ξ if and only if $|B| \le A$, i.e., $-A \le B \le A$. In our case $A > 1$, then Method (5) is linearly, unconditionally stable.

Method (5) is implicit, hence a nonlinear equation should be solved for the calculation of U_m^{n+1} from U_m^n, and U_m^{n-1}. We use Newton's iterative method given by

$$U_m^{(k+1)} - 2\,U_m^n + U_m^{n-1} - \Delta t^2\,\mathcal{A}(\mathrm{E})\,\frac{(U_m^{(k+1)} + U_m^{n-1})}{2} + \Delta t^2\,\left(H(U_m^{(k)}) + H_u(U_m^{(k)})\,(U_m^{(k+1)} - U_m^{(k)})\right) = 0, \tag{7}$$

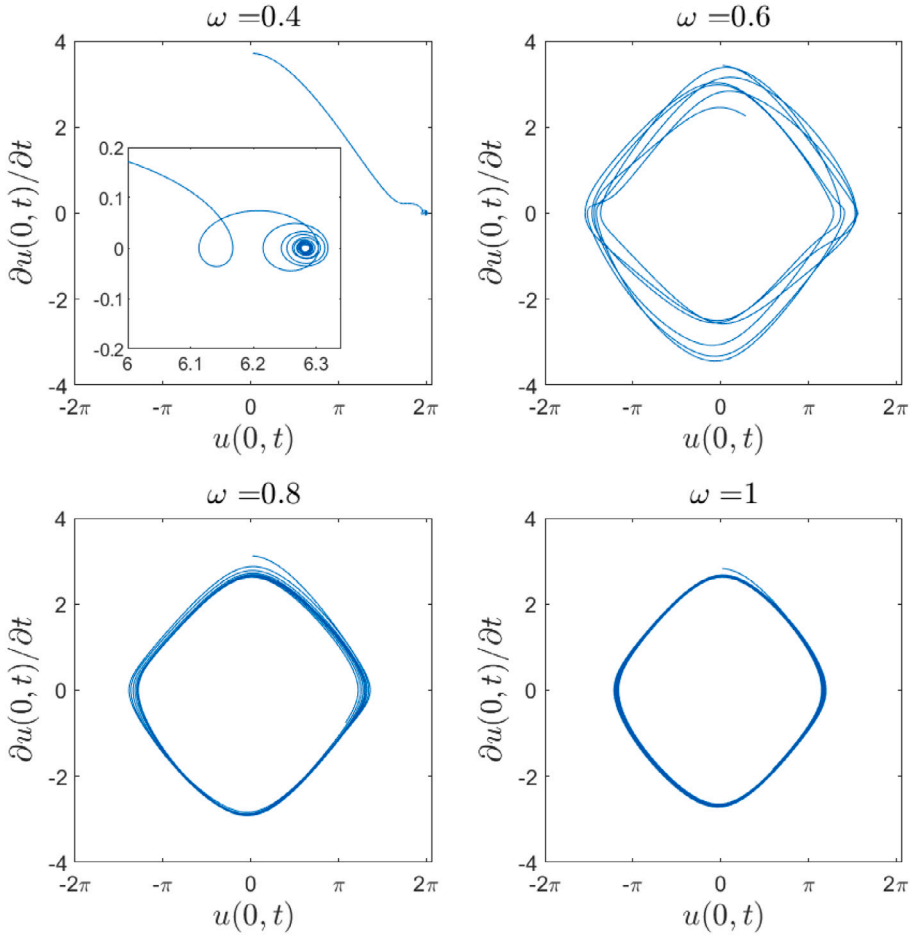

Fig. 3. Phase diagrams ($u(0,t)$ vs. $u_t(0,t)$) for the numerical solutions of the GSL equation with $b = 1$ shown in Fig. 2.

with

$$H_u(U_m^{(k)}) \equiv \frac{G_u(U_m^{(k)})\,(U_m^{(k)} - U_m^{n-1}) - (G(U_m^{(k)}) - G(U_m^{n-1}))}{\left(U_m^{(k)} - U_m^{n-1}\right)^2}. \tag{8}$$

In each interaction of the Newton's method the linear problem

$$\mathcal{M}^{(k)}\, U_m^{(k+1)} = \mathcal{B}^{(k)},$$

where the matrix $\mathcal{M}^{(k)}$ is given by

$$\mathcal{M}^{(k)} = \mathcal{I} - \frac{\Delta t^2}{2}\,\mathcal{A} + \Delta t^2\, H_u(U_m^{(k)}), \tag{9}$$

with $\mathcal{I}$ the identity matrix and $\mathcal{A}$ the matrix associated to the finite difference operator $\mathcal{A}(E)$, and the vector $\mathcal{B}^{(k)}$ is

$$\mathcal{B}^{(k)} = 2\,U_m^n - U_m^{n-1} + \frac{\Delta t^2}{2}\,\mathcal{A}\,U_m^{n-1} - \Delta t^2\,\left(H(U_m^{(k)}) - H_u(U_m^{(k)})\,U_m^{(k)}\right). \tag{10}$$

Our stopping criterium for Newton's iteration convergence is based on the relative error using the infinity norm, i.e., $\|U_m^{(k+1)} - U_m^{(k)}\|_\infty \le \mathrm{Tol}_{\mathrm{rel}}\,\|U_m^{(k+1)}\|_\infty$, with $\|U_m^{(k)}\|_\infty = \max_m |U_m^{(k)}|$, and $\mathrm{Tol}_{\mathrm{rel}} = 10^{-14}$.

The pseudocode of our implementation of Method (5) is presented in Algorithm 1. This pseudocode calculates the numerical solution U_m^n in matrix form. Let us note that the initial condition $u_b(x,t)$ in this pseudocode corresponds to the pseudo-breather to be presented in the next section, cf. Eq. (14).

Let us emphasize that Method (5) is highly accurate and has excellent energy conservation properties, even for $\Delta t = \Delta x$, as shown by these authors for the sG equation in Ref. [30]. Our extensive simulations show that these properties hold for the GSL equation as well.

Algorithm 1 Pseudocode of the implementation of Method (5)

```
U_m^0 ← 0
U_m^{-1} ← u_b(x_m, −Δt)                          ▷ Initial condition
n ← 0
while n < t_max/Δt do                              ▷ Main loop
    U_m^(k) ← 0
    U_m^(k+1) ← U_m^n
    while ‖U_m^(k+1) − U_m^(k)‖_∞ > Tol_rel ‖U_m^(k+1)‖_∞ do   ▷ Newton's loop
        U_m^(k) ← U_m^(k+1)
        Calculate matrix M^(k) and vector B^(k)
        U_m^(k+1) ← Solution of linear system M^(k) U_m^(k+1) = B^(k)
    end while
    U_m^{n+1} ← U_m^(k+1)
    n ← n + 1
end while
```

2.2. Initial condition for searching the quasi-breather

The initial conditions for our numerical method are $U_m^{-1} = u(x_m, -\Delta t)$, and $U_m^0 = u(x_m, 0)$. The sine-Gordon breather can be written as

$$u_{\mathrm{br}}(x,t) = 4\,\tan^{-1}(\mathrm{sech}(q\,x)\,\sin(\omega\,q\,t)/\omega), \qquad q = 1/\sqrt{1+\omega^2}. \tag{11}$$

Here on, the parameter ω is referred to as frequency, although the breather frequency $\omega_{\mathrm{br}}(\omega) = \omega/\sqrt{1+\omega^2}$. Eq. (11) has the advantage that $u_{\mathrm{br}}(x,0) = 0$, so $U_m^0 = u_{\mathrm{br}}(x_m,0) = 0$ is an exact initial condition for the GSL equation. Moreover, since $u_{\mathrm{br}}(x,t) = 4\,q\,\mathrm{sech}(q\,x)\,t + O\left(t^3\right)$,

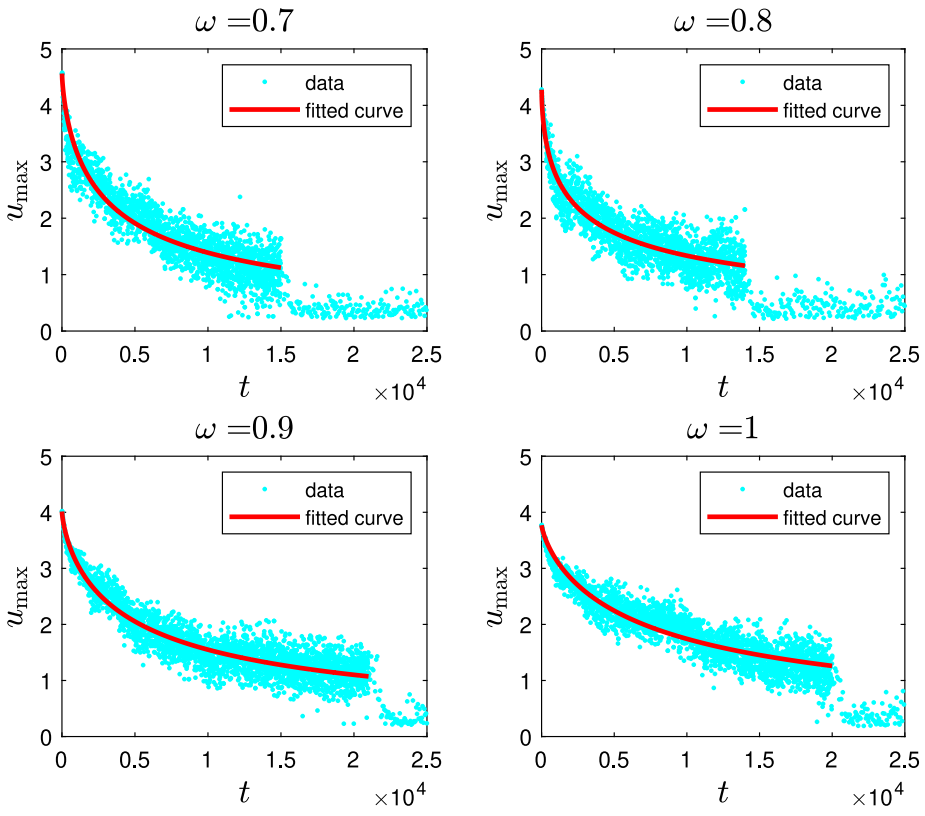

Fig. 4. Plots of the quasi-breather amplitude maxima $u_{\max}(t_i)$ (cyan points) and its fitting (red line) by Eq. (16) with $t_i \le T_{\max}$ (see Table 1) for $\omega = 0.7$ (top left), 0.8 (top right), 0.9 (bottom left plot), and 1 (bottom right), with $b = 1$, $\Delta t = \Delta x = 0.01$, $x \in [-50, 50)$, and $t \in [0, 25000]$. (For interpretation of the references to colour in this figure legend, the reader is referred to the web version of this article.)

an asymptotic expansion in time can be used to obtain an accurate approximation $U_m^{-1} = u(x_m, -\Delta t)$ for the GSL equation. The introduction of the ansatz

$$u_b(x,t) = 4\,q\ \mathrm{sech}(q\,x)\,t + u_3(x)\,t^3 + u_5(x)\,t^5 + u_7(x)\,t^7 + O\left(t^9\right), \tag{12}$$

into the GSL equation yields

$$(4\ \mathrm{sech}(q\,x)\,(q - q^3 + 2\,q^3\ \mathrm{sech}^2(q\,x)) + 6\,u_3(x))\,t = O\left(t^3\right), \tag{13}$$

where $u_3(x)$ can be trivially solved. The repetition of this procedure to higher orders in time yields the regular asymptotic expansion

$$\begin{aligned} u_b(x,t) = {} & 4\,t\,q\ \mathrm{sech}(q\,x) - \frac{2\,t^3}{3}\,q\ \mathrm{sech}(q\,x)\left(1 - q^2 + 2\,q^2\ \mathrm{sech}^2(q\,x)\right) \\ & + \frac{t^5}{30}\left(q\,(1-q^2)^2\,\mathrm{sech}(q\,x) + 4\,q^3\,(5 + 6\,b^2 - 5\,q^2)\ \mathrm{sech}^3(q\,x)\right. \\ & \left. + 24\,q^5\ \mathrm{sech}^5(q\,x)\right) \\ & - \frac{t^7}{1260}\left(q\,(1-q^2)^3\ \mathrm{sech}(q\,x) + 2\,q^3\ \left(b^2\,(132 - 228\,q^2)\right.\right. \\ & \left. + 91\,(1-q^2)^2\right)\ \mathrm{sech}^3(q\,x) + 24\,q^5\ \left(8\,b^2\,(14 + 15\,b^2)\right. \\ & \left.\left. - 35\,(1-q^2)\right)\ \mathrm{sech}^5(q\,x) + 720\,q^7\ \mathrm{sech}^7(q\,x)\right) \\ & + O\left(t^9\right), \end{aligned} \tag{14}$$

which can be used for the initial condition $U_m^{-1} = u_b(x_m, -\Delta t)$. Note that for $\Delta t \le 0.01$, $q < 1$, and $b \le 1$, the $O\left(t^9\right)$ term in Eq. (14) is smaller than the epsilon of the machine (2.2×10^{-16}); however, for $b \gg 1$ high-order terms in Eq. (14) are required in order to obtain an accurate initial condition.

The energy associated to the solution Eq. (14) can be analytically calculated as

$$E(t) = \int_{-\infty}^{\infty}\left(\frac{(u_{b,t})^2}{2} + \frac{(u_{b,x})^2}{2} + G(u_b)\right)dx$$

$$= E(0) = \int_{-\infty}^{\infty} 8\,q^2\,\mathrm{sech}^2(qx)\,dx = \frac{16}{\sqrt{1+\omega^2}}. \tag{15}$$

Note that this energy is independent of the parameter b, hence it coincides with that of the sine-Gordon breather, given by Eq. (11).

3. Presentation of results

Let us summarize the main results for the behaviour of the GSL equation, obtained after a large set of simulations. In Section 3.1, the different solutions obtained as the frequency of the initial condition increases are characterized. In Section 3.2, the evolution in time of the parameters of the quasi-breather solutions is presented. And in Section 3.3 the long-time stability of the quasi-breather is analysed.

3.1. Kink-antikink, pseudo-breather, and quasi-breather solutions

The numerical solution of the sine-Gordon equation, i.e., the GSL equation with $b = 0$, with the initial condition (14) results in the exact breather solution for every value of the frequency ω (or m). However, extensive numerical simulations for the GSL equation with $b > 0$ show that there is a critical minimum frequency ω_{cr} such that the solution evolves into a kink-antikink solution for $\omega < \omega_{\mathrm{cr}}$ and into a quasi-breather for $\omega > \omega_{\mathrm{cr}}$. This result is illustrated in the three-dimensional mesh plots in Fig. 1, where the GSL equation with $b = 1$ is solved with initial condition (14) for $\omega = 0.4$ (top left plot), 0.6 (top right plot), 0.8 (bottom left plot), and 1.0 (bottom right plot). The top left plot ($\omega = 0.4$, $q = 5/\sqrt{29}$) shows the generation of a kink and antikink that separate completely and escape to infinity. The top right plot ($\omega = 0.6$, $q = 5/\sqrt{34}$) shows the generation of a periodic solution that resembles a quasi-breather, but with noticeable variations in the profile of its amplitude in every oscillation period; here on, it is referred to as a pseudo-breather. Both, the bottom left plot ($\omega = 0.8$, $q = 5/\sqrt{41}$) and

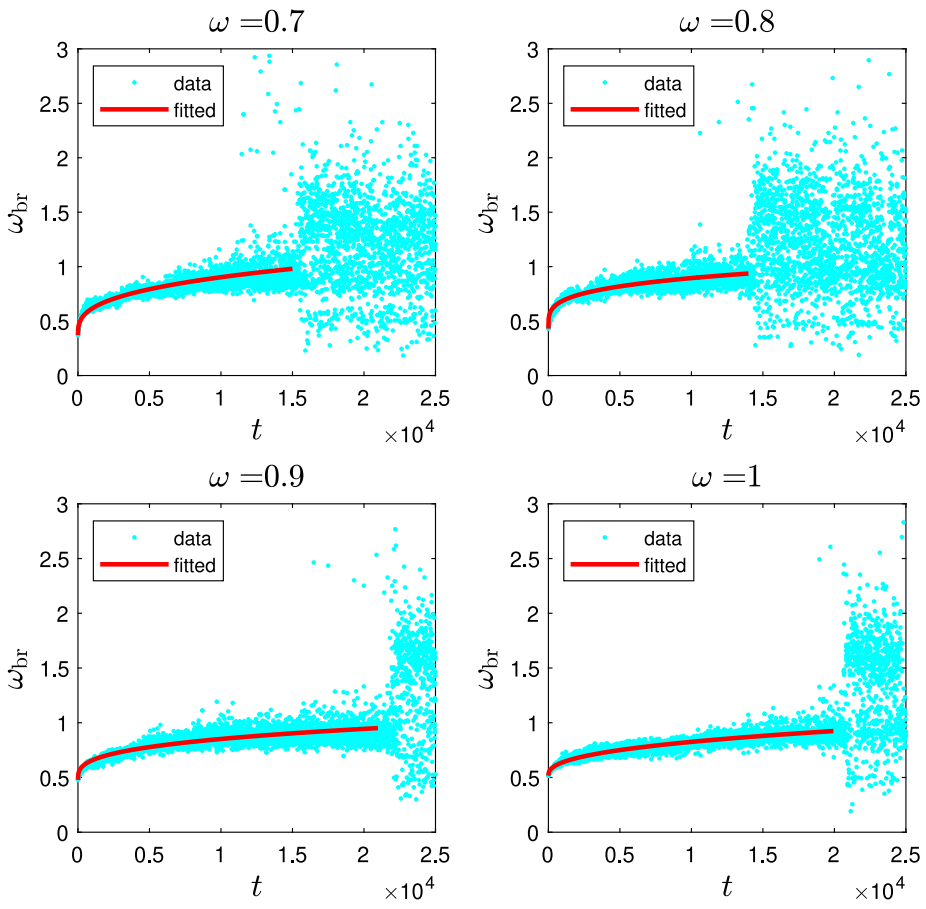

Fig. 5. Plots of the quasi-breather frequencies $\omega_{\rm qbr}(t_i)$ (cyan points) and its fitting (red line) by Eq. (17) for $t_i \leq T_{\rm max}$ (see Table 1) for $\omega = 0.7$ (top left), 0.8 (top right), 0.9 (bottom left plot), and 1 (bottom right), with $b = 1$, $\Delta t = \Delta x = 0.01$, $x \in [-50, 50)$, and $t \in [0, 25000]$. (For interpretation of the references to colour in this figure legend, the reader is referred to the web version of this article.)

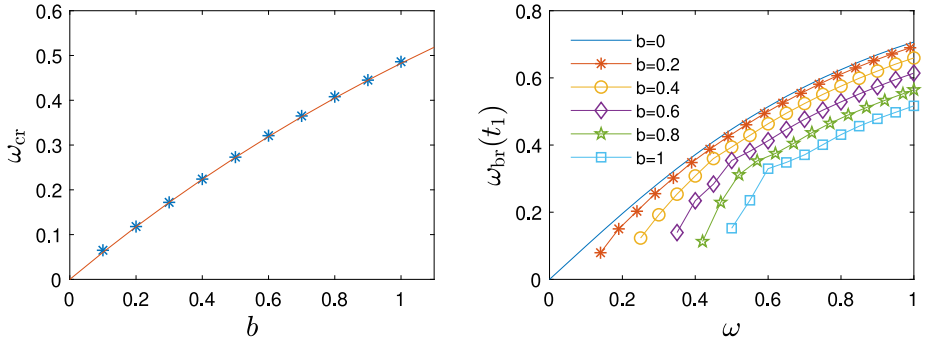

Fig. 6. The left plot shows the critical frequency $\omega_{\rm cr}$ as function of b estimated from numerical calculations and its fitting by Eq. (18). The right plot shows the first quasi-breather frequency $\omega_{\rm qbr}(t_1)$ for $b = 0.2$, 0.4, 0.6, 0.8, and 1 as a function of ω, and the breather frequency $\omega_{\rm br}(\omega)$ for the sG equation (continuous line). All the simulations use $\Delta t = \Delta x = 0.01$, $x \in [-50, 50)$, and $t \in [0, 100]$.

the bottom right plot ($\omega = 1.0$, $q = 1/\sqrt{2}$) show quasi-breather solutions with nearly constant amplitude and frequency; as the parameter ω increases, the frequency of the quasi-breather also increases. The four plots in Fig. 1 show solutions emitting small-amplitude radiation with a small amplitude that slowly increases as time passes since the radiation reenters the domain due to the periodic boundary conditions.

Fig. 2 shows plots of $u(0, t)$ for the solutions shown in Fig. 1 in order to illustrate the profile of the corresponding kink-antikink, pseudo-breather, and quasi-breather solutions. The top left plot ($\omega = 0.4$) shows that the amplitude in the centre of the kink-antikink solution increases from 0 to 2π, with a small ripple whose amplitude decreases in time. The top right plot ($\omega = 0.6$) shows the central profile of the pseudo-breather, whose profile in every period changes appreciably both in amplitude and frequency. The bottom left plot ($\omega = 0.8$, $q = 5/\sqrt{41}$) and the bottom right plot ($\omega = 1.0$, $q = 1/\sqrt{2}$) show the central profile of quasi-breather solutions with nearly constant amplitude and frequency. A careful analysis of the quasi-breather profiles concludes that the amplitude (frequency) decreases (increases) in a small amount as time passes due to the slow emission of radiation (not noticeable in these plots).

Fig. 3 shows phase plots, i.e., $u(0, t)$ vs $u_t(0, t)$, for the solutions shown in Fig. 2 in order to highlight the quality of the profiles of the quasi-breathers and the effect of the radiation. The phase portrait of the

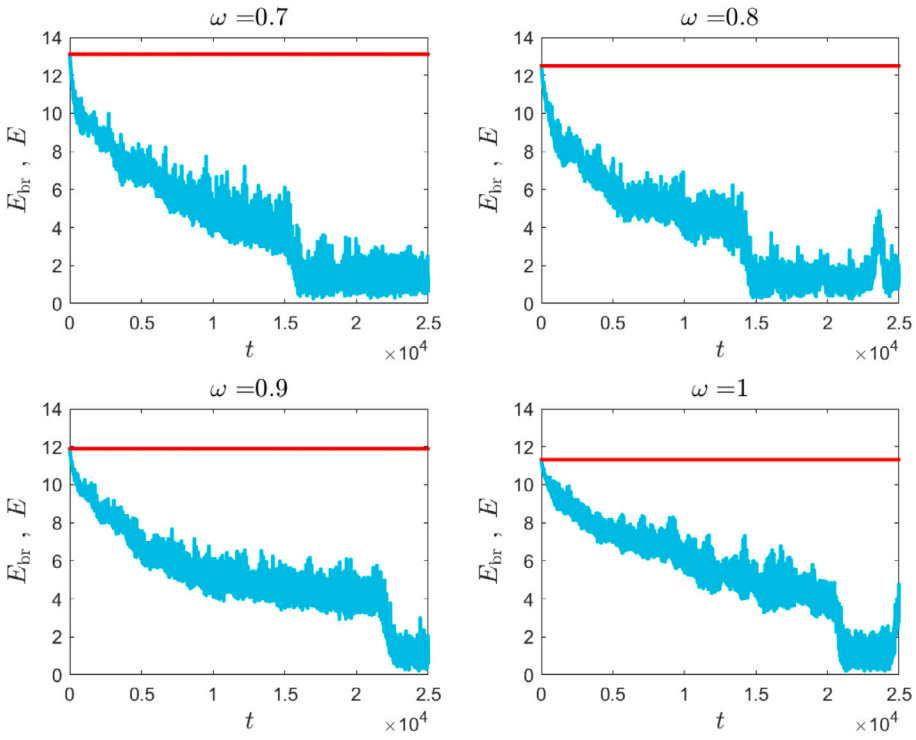

Fig. 7. Plots of the energy of the quasi-breather $E_{\rm qbr}(t)$ (blue points) and the total energy $E(t)$ (red line) for $\omega = 0.7$ (top left), 0.8 (top right), 0.9 (bottom left plot), and 1 (bottom right), with $b = 1$, $\Delta t = \Delta x = 0.01$, $x \in [-50, 50)$, and $t \in [0, 25000]$. (For interpretation of the references to colour in this figure legend, the reader is referred to the web version of this article.)

Table 1
The parameters of Eq. (16) for the local maxima of the quasi-breather shown in the plots of Fig. 4; α and γ are fitted from data in $t \in [0, T_{\rm max}]$, with fixed values for $T_{\rm max}$ and t_1; the values of α and γ are shown with the corresponding 95% confidence intervals and the coefficient of determination R^2.

ω	t_1	$u_{\rm max}(t_1)$	$T_{\rm max}$	α	γ	R^2
0.7	3.94	4.5640	15 000	0.0030 ± 0.0004	0.72 ± 0.02	0.82
0.8	3.47	4.2775	14 000	0.0089 ± 0.0013	0.60 ± 0.02	0.77
0.9	3.19	4.0146	21 000	0.0018 ± 0.0002	0.73 ± 0.01	0.86
1.0	2.98	3.7694	20 000	0.0009 ± 0.0001	0.77 ± 0.01	0.85

Table 2
The parameters of Eq. (17) for the frequency of the quasi-breather shown in the plots of Fig. 5. The parameters $\tilde{\alpha}$ and $\tilde{\gamma}$ are fitted from data in $t \in [0, T_{\rm max}]$, with t_1 and $T_{\rm max}$ as fixed parameters; being the values of $T_{\rm max}$ the same shown in Table 1. The values of $\tilde{\alpha}$ and $\tilde{\gamma}$ are shown with the corresponding 95% confidence intervals and the coefficient of determination R^2.

ω	t_1	$\omega_{\rm qbr}(t_1)$	$\omega_{\rm br}(\omega)$	$\tilde{\alpha}$	$\tilde{\gamma}$	R^2
0.7	3.94	0.3709	0.5735	0.066 ± 0.015	0.335 ± 0.025	0.35
0.8	3.47	0.4309	0.6247	0.099 ± 0.013	0.258 ± 0.015	0.47
0.9	3.19	0.4782	0.6689	0.041 ± 0.006	0.319 ± 0.016	0.47
1.0	2.98	0.5167	0.7071	0.015 ± 0.002	0.402 ± 0.016	0.61

quasi-breather is an open oscillatory profile resembling the limit cycle of the breather of the sine-Gordon equation. The top left plot ($\omega = 0.4$) shows that the solution starts approaching the expected phase portrait for a quasi-breather, but deviates as $u_t(0, t)$ approaches zero, making a transition with two loops into a spiral sink around $u(0, t) = 2\pi$ and $u_t(0, t) = 0$, as clearly shown in the zoomed plot inserted. The top right plot ($\omega = 0.6$) shows the phase portrait of a periodic solution with an irregular profile different from the one expected for a quasi-breather. Both, the bottom left plot ($\omega = 0.8$, $q = 5/\sqrt{41}$) and the bottom right plot ($\omega = 1.0$, $q = 1/\sqrt{2}$) show the central profile of quasi-breather solutions with nearly constant amplitude and frequency.

3.2. Properties of the quasi-breather solution

The maximum amplitude $u_{\rm max}(t_i)$, $i = 1, 2, \ldots$, of the oscillatory profile $u(0, t)$ of the quasi-breather decreases as time marches due to the emission of radiation, until the quasi-breather loses its identity decaying into small-amplitude radiation at a time $t = T_{\rm max}$. Fig. 4 shows $u_{\rm max}(t_i)$ of the quasi-breather of the GSL equation with $b = 1$ for $\omega = 0.7$, 0.8, 0.9, and 1, from a long-time numerical integration until $t = 25000$. This figure shows a sharp transition between a decaying quasi-breather and a small-amplitude radiation solution at time $t \approx T_{\rm max}$. The values of $u_{\rm max}(t_i)$, $i = 1, 2, \ldots, N$, with $t_N \leq T_{\rm max}$ have been fitted by the expression

$$u_{\rm max}(t) = \frac{u_{\rm max}(t_1)}{1 + \alpha (t - t_1)^{\gamma}}, \tag{16}$$

where the first data point $(t_1, u_{\rm max}(t_1))$ has been fixed in order to enforce that Eq. (16) exactly passes for such a point. Table 1 shows the values of the fixed parameters t_1, $u_{\rm max}(t_1)$, and $T_{\rm max}$, and the fitted parameters α and γ with 95% confidence intervals for $\omega = 0.7$, 0.8, 0.9, and 1; the coefficient of determination R^2 is shown in the table, being larger than 0.77 in the four cases. Fig. 4 and Table 1 show that t_1 and $u_{\rm max}(t_1)$ decrease as ω grows; the behaviour of $T_{\rm max}$ is irregular, although the general trend is to increase as ω does. Table 1 shows that the fitted coefficient α decreases and γ increases as ω grows, except for $\omega = 0.8$.

The quasi-breather frequency $\omega_{\rm qbr}(t_i) = 2\pi/(t_{i+1} - t_i)$ has been calculated from the local maxima $(t_i, u_{\rm max}(t_i))$ of the oscillatory profile $u(0, t)$; note that, after the decay of the quasi-breather, $t > T_{\rm max}$, this frequency corresponds to that of the small-amplitude radiation, so it oscillates widely. Fig. 5 shows $\omega_{\rm qbr}(t_i)$ of the GSL equation with $b = 1$ for $\omega = 0.7$, 0.8, 0.9, and 1, from a long-time numerical integration until $t = 25000$. This figure shows that $\omega_{\rm qbr}(t_i)$ increases as time marches, with $t < T_{\rm max}$. The values of $\omega_{\rm qbr}(t_i)$, $i = 1, 2, \ldots, N$, with $t_N \leq T_{\rm max}$ have been fitted by the expression

$$\omega_{\rm qbr}(t) = \omega_{\rm qbr}(t_1)\,(1 + \tilde{\alpha}\,(t - t_1)^{\tilde{\gamma}}, \tag{17}$$

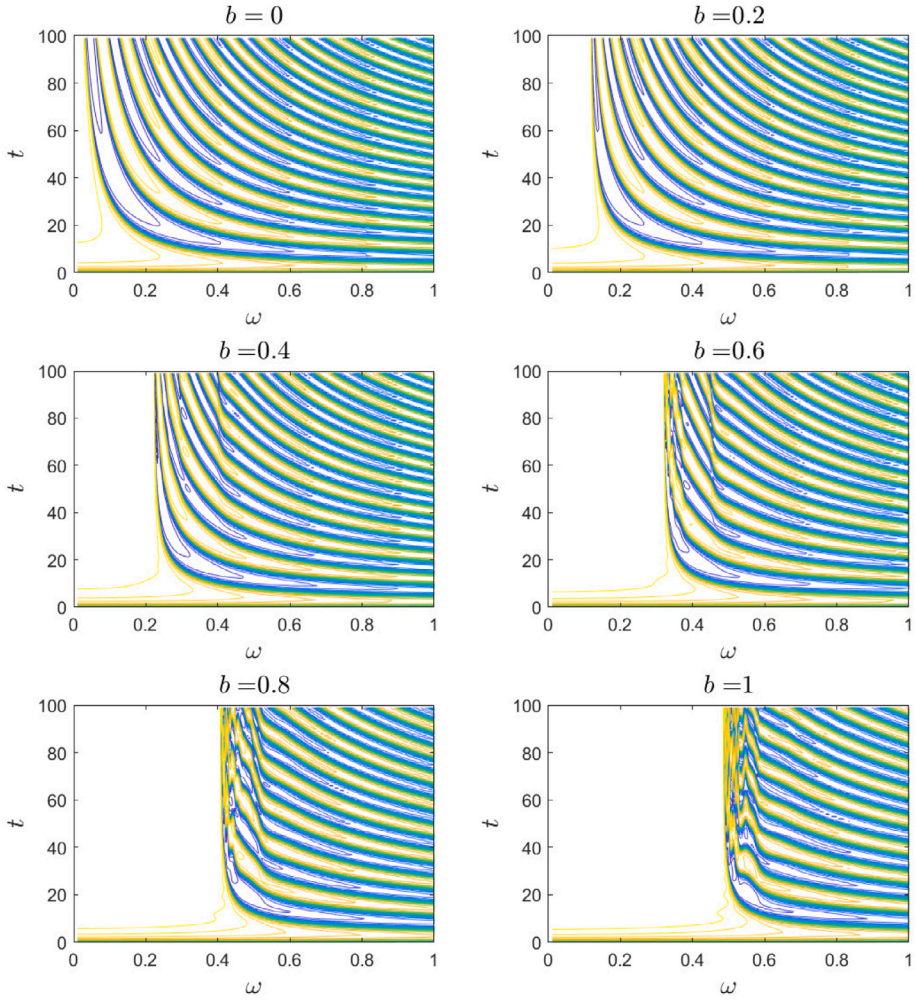

Fig. 8. Contour plots of the quasi-breather solution $u(0,t)$ in the plane (ω,t) with $\omega \in [0,1]$ in steps of $\Delta\omega = 10^{-3}$, for $b = 0$, 0.2, 0.4, 0.6, 0.8, and 1, with $\Delta t = \Delta x = 0.01$, $x \in [-50,50)$, and $t \in [0,100]$.

where the first data point $(t_1, \omega_{\rm qbr}(t_1))$ has been fixed in order to enforce that Eq. (17) exactly passes for such a point. Table 2 shows the values of the fixed parameters t_1 and $\omega_{\rm qbr}(t_1)$, and the fitted parameters $\tilde{\alpha}$ and $\tilde{\gamma}$ with 95% confidence intervals for $\omega = 0.7$, 0.8, 0.9, and 1; the coefficient of determination R^2 for this fitting is smaller than 0.61 for $\omega < 1$ due to the presence of values of $\omega_{\rm qbr} > 2$ for t approaching $T_{\rm max}$. Fig. 5 and Table 2 show that $\omega_{\rm qbr}(t_1)$ increases as ω does, starting with $\omega_{\rm qbr}(t_1) < \omega/\sqrt{1+\omega^2}$, the frequency of the breather of the sG equation, but reaching a time after which $\omega_{\rm qbr}(t_i) > \omega/\sqrt{1+\omega^2}$. Table 2 shows that the fitted coefficient $\tilde{\alpha}$ decreases as ω grows, except for $\omega = 0.8$, and $\tilde{\gamma}$ increases as ω grows, except for $\omega = 0.7$.

Fig. 6 (left plot) shows the critical frequency $\omega_{\rm cr}$ as function of b, showing that it is monotonically increasing. The data points can be fitted by an exponential function

$$\omega_{\rm cr}(b) = \tilde{\alpha}\,(1 - \exp(-\tilde{\beta}\, b)), \tag{18}$$

resulting in

$$\tilde{\alpha} = 1.19^{+0.09}_{-0.08}, \qquad \tilde{\beta} = 0.52^{+0.05}_{-0.04}, \tag{19}$$

both with 95% confidence intervals and a coefficient of determination $R^2 = 0.9999$. Fig. 6 (right plot) shows the breather frequency $\omega_{\rm br}(\omega)$ for the sG equation $b = 0$ (continuous line), and the first quasi-breather frequency $\omega_{\rm qbr}(t_1)$ for $b = 0.2$, 0.4, 0.6, 0.8, and 1 as a function of ω; this plot shows the first quasi-breather frequency $\omega_{\rm qbr}(t_1)$ as a function of ω for $b = 0, 0.2, \ldots, 1$. The values of $\omega_{\rm qbr}(t_1)$ increase as ω does and decrease as b increases, but always are smaller than the frequency $\omega_{\rm br}(\omega)$ of the sG breather. Fig. 6 (right plot) shows that $\omega_{\rm qbr}(t_1)(\omega)$ approaches $\omega_{\rm br}(\omega)$, as expected since the quasi-breather of the GSL equation can be interpreted as a perturbation of the breather of the sG equation, at least for small b. For this reason $\omega_{\rm qbr}(t_1)(\omega)$ is an increasing function of ω as $\omega_{\rm br}(\omega)$ does.

The energy of the (stationary) quasi-breather can be estimated by using

$$E_{\rm qbr}(t) = \int_{-2\pi}^{2\pi} \left(\frac{(u_t)^2}{2} + \frac{(u_x)^2}{2} + G(u) \right) dx \le E(t), \tag{20}$$

where $E_{\rm qbr}(0) \approx E(0)$, since the initial condition $u_b(x,0)$ exponentially decays in space. Fig. 7 shows $E_{\rm qbr}(t)$ (blue points) and $E(t)$ (red line) for $\omega = 0.7$ (top left), 0.8 (top right), 0.9 (bottom left plot), and 1 (bottom right), with $b = 1$. Since our numerical method has good energy-conservation properties, the energy is nearly constant; in fact, there is a small increase in $E(t)$ as time marches, but since $|E(25000)/E(0) - 1| < 7.5 \times 10^{-5}$ for all ω, it is not noticeable in the plots. Fig. 7 shows that $E_{\rm qbr}(t)$ decreases as the quasi-breather radiates for $t < T_{\rm max}$; after a sharp decrease, it finally decays into small-amplitude radiation.

3.3. Critical frequency for the quasi-breather solution

Fig. 8 shows contour plots of the solution $u(0,t)$ in the plane (ω,t), with $\omega \in [0,1]$ in steps of $\Delta\omega = 10^{-3}$, for the numerical solution of Eq. (2) with $b = 0$, 0.2, 0.4, 0.6, 0.8, and 1. The top left plot for $b = 0$ shows the analytical breather solution, Eq. (11), of the sG equation; it

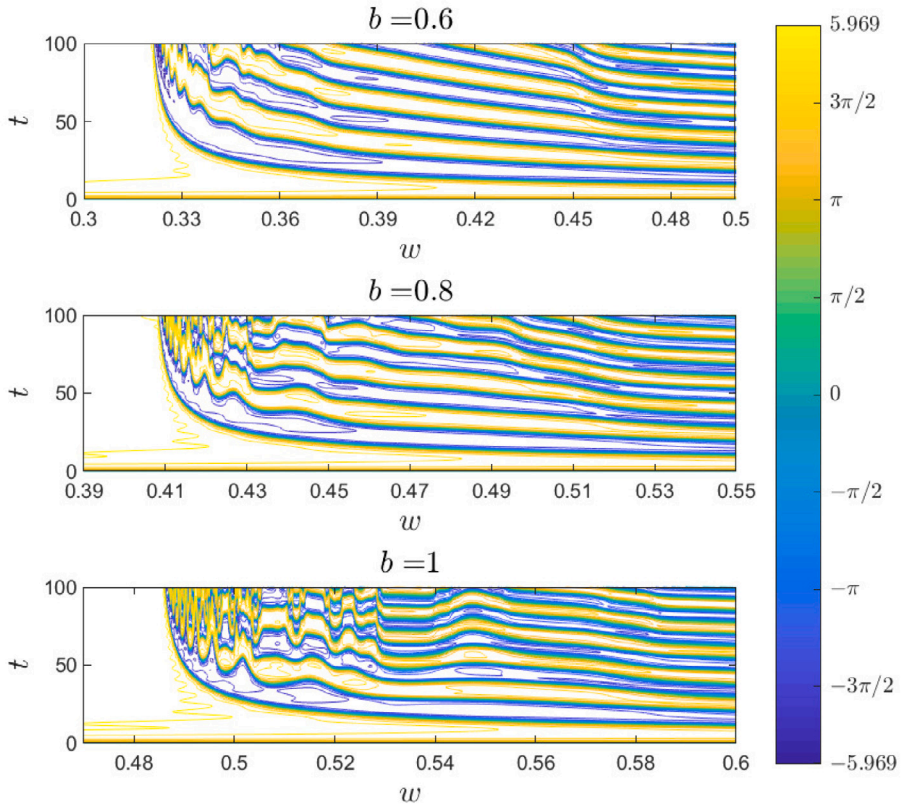

Fig. 9. Zoom of the contour plots of the quasi-breather solution $u(0,t)$ in the plane (ω,t) with $\Delta\omega = 10^{-4}$ for $b = 0.6$ in $\omega \in [0.3, 0.5]$, for $b = 0.8$ in $\omega \in [0.39, 0.55]$, and $b = 1$ in $\omega \in [0.47, 0.6]$, using $\Delta t = \Delta x = 0.01$, $x \in [-50, 50)$, and $t \in [0, 100]$.

Table 3
Critical frequencies ω_{cr} and $\omega_{cr,br}$ for $b = 0, 0.2, \ldots, 1$, determined from the simulations plotted in Figs. 8 and 9.

b	0	0.2	0.4	0.6	0.8	1.0
ω_{cr}	0	0.118	0.224	0.321	0.408	0.486
$\omega_{cr,br}$	0	0.118	0.40	0.46	0.53	0.59

clearly shows that the frequency of the breather increases as ω does, as expected from $\omega_{br}(\omega) = \omega/\sqrt{1+\omega^2}$. The other five plots for $b > 0$ in Fig. 8 clearly show the existence of two critical frequencies, ω_{cr}, such that the solution evolves into a kink-antikink solution for $\omega < \omega_{cr}$ and $\omega_{cr,br}$, such that the solution is a quasi-breather for $\omega > \omega_{cr,br}$, but an irregular solution for $\omega_{cr} < \omega < \omega_{cr,br}$, as illustrated for $b = 1$ in the three-dimensional mesh plots in Fig. 1; the values of ω_{cr} and $\omega_{cr,br}$ for $b = 0, 0.2, \ldots, 1$, are shown in Table 3. The top right plot for $b = 0.2$ shows that the contour plot of the numerical quasi-breather for $\omega > \omega_{cr}$ is very similar to that of the breather for $\omega > 0$ (top left plot); however, the slope of the contours for $\omega \gtrsim \omega_{cr}$ for $b = 0.2$ is larger than for $\omega \gtrsim 0$ for $b = 0$. The middle left plot for $b = 0.4$ shows a new feature in the contour plot with respect to that for $b = 0.2$ (top right plot), a change of the contours' slope around $\omega_{cr,br}$; such a feature is also shown in the middle right plot ($b = 0.6$). The bottom left plot for $b = 0.8$ and the bottom right plot for $b = 1$ show, for $\omega_{cr} < \omega < \omega_{cr,br}$, an irregular behaviour in both amplitude and frequency of the oscillatory solution, including several slope changes in the contour plots, here on referred to as a pseudo-breather.

In order to highlight the features of the pseudo-breather for $\omega_{cr} < \omega < \omega_{cr,br}$, Fig. 9 shows contour plots of the solution $u(0,t)$ for $b = 0.6$, 0.8, and 1 with smaller resolution in frequency, $\Delta\omega = 10^{-4}$, than that used in Fig. 8, cf. $\Delta\omega = 10^{-3}$. The top plot for $b = 0.6$ shows that the contours of the solution present irregular fluctuations for $\omega_{cr} < \omega < 0.36$, and two changes in the slope of the contours near $\omega = 0.37$ and 0.46; there are no slope changes for $\omega > \omega_{cr,br}$. The middle plot for $b = 0.8$ shows highly irregular oscillations for $\omega_{cr} < \omega < 0.43$; there are several slope changes in the interval $0.43 < \omega < \omega_{cr,br}$, where a pseudo-breather is observed. Finally, the bottom plot for $b = 1$ also shows highly irregular oscillations for $\omega_{cr} < \omega < 0.53$ and several slope changes in the interval $0.53 < \omega < \omega_{cr,br}$. Our numerical experiments show that the pseudo-breather is a short-lived oscillatory solution, in contrast to the long-lived quasi-breather.

4. Conclusions

A numerical search for the stationary quasi-breather solution of the graphene superlattice equation has been undertaken. A fourth-order in space, second-order in time, energy-conserving, finite difference method has been used. This method is applicable to other nonlinear Klein–Gordon equations and, even, with proper changes, to nonlinear wave equations with fractional time derivatives [34,35].

We have used a new initial condition for the quasi-breather search, instead of the standard initial condition for the same task that uses a singular perturbation of the breather solution of the sine-Gordon equation with its maximum amplitude at the starting time. We have used a null initial condition whose derivative in time is calculated by means of a regular asymptotic expansion with the breather of the sine-Gordon as an ansatz. An advantage of such an initial condition is that it is very accurate for a small enough time step, so the initial emission of radiation during the quasi-breather development is reduced. Another advantage is that the total energy of the solution can be calculated exactly.

The numerical results show that the initial condition evolves into three possible solutions depending on its frequency ω, a kink-antikink solution for $\omega < \omega_{cr}$, a pseudo-breather for $\omega_{cr} < \omega < \omega_{cr,br}$, and a quasi-breather solution for $\omega > \omega_{cr,br}$. The pseudo-breather is an irregular oscillatory solution, unlike the regular oscillations of

the quasi-breather. This is the first report on the existence of two critical frequencies ω_{cr} and $\omega_{cr,br}$ for the breather-like solutions of a modification of the sine-Gordon equation.

Long-time simulations show that the quasi-breather for $\omega > \omega_{cr,br}$ survives for more than one thousand periods (the number depends on b and the frequency ω in the initial condition), although its amplitude and energy decrease, and its frequency increases. In order to evaluate the robustness of the quasi-breather solution, we have introduced a new contour plot inspired by the corresponding plot used to study the fractal structure of the kink-antikink collisions. This new plot highlights the existence of the two critical frequencies and allows an easy comparison of the quasi-breather solution as a function of any free parameter in the modification of the sine-Gordon equation (in our case the geometrical parameter b of the graphene superlattice equation).

The study of moving quasi-breathers, their mutual collisions, and their collisions with kinks and antikinks in the graphene superlattice equation is a future research line; from the practical point of view, they could have a significant role in the bandgap engineering in graphene [36]. The relation between the quasi-breathers and the breather-like solutions observed in the fusion of a kink-antikink pair also deserves a detailed study. Moreover, our results support the experimental search for the quasi-breather solution in real graphene superlattice devices; for this task, it is necessary to study the most suitable profiles for the input signal to be injected into the device in order to sustain a quasi-breather during a large number of periods. Finally, the quasi-breathers of the integro-differential equation introduced by Kryuchkov, Kukhar', and Zav'yalov [37] for the modelling of terahertz electromagnetic waves in the graphene superlattice also is an interesting line for further research.

Declaration of competing interest

The authors declare the following financial interests/personal relationships which may be considered as potential competing interests: Francisca Martin-Vergara, Francisco Rus and Francisco R. Villatoro reports financial support was provided by University of Malaga.

Francisca Martin-Vergara, Francisco Rus and Francisco R. Villatoro reports a relationship with University of Malaga that includes: employment.

Data availability

No data was used for the research described in the article.

Acknowledgements

The authors thank the reviewers for their thoughtful comments and efforts toward improving our manuscript. The research reported here was supported by Project RoCoSoyCo (UMA18-FEDERJA-248) of the Consejería de Economía y Conocimiento, Junta de Andalucía, Spain.

References

[1] Kryuchkov SV, Kukhar' EI. The solitary electromagnetic waves in the graphene superlattice. Physica B 2013;408:188–92. http://dx.doi.org/10.1016/j.physb.2012.09.052.

[2] Ratnikov P. Superlattice based on graphene on a strip substrate. JETP Lett 2009;90:469–74. http://dx.doi.org/10.1134/S0021364009180143.

[3] Martin-Vergara F, Rus F, Villatoro FR. Solitary waves on graphene superlattices. In: Archilla JFR, Palmero F, Lemos MC, Sánchez-Rey B, Casado-Pascual J, editors. Nonlinear systems, Vol. 2. Nonlinear phenomena in biology, optics and condensed matter. Berlin: Springer; 2018, p. 85–110. http://dx.doi.org/10.1007/978-3-319-72218-4_4.

[4] Azadi L, Shojaei S. Optical absorption in planar graphene superlattice: The role of structural parameters. Superlattices Microstruct 2018;116:95–104. http://dx.doi.org/10.1016/j.spmi.2018.02.007.

[5] Yan H, Chu Z-D, Yan W, Liu M, Meng L, Yang M, Fan Y, Wang J, Dou R-F, Zhang Y, Liu Z, Nie J-C, He L. Superlattice Dirac points and space-dependent Fermi velocity in a corrugated graphene monolayer. Phys Rev B 2013;87:075405. http://dx.doi.org/10.1103/PhysRevB.87.075405.

[6] Lu J, Zhang K, Feng Liu X, Zhang H, Chien Sum T, Castro Neto AH, Loh KP. Order–disorder transition in a two-dimensional boron–carbon–nitride alloy. Nature Commun 2013;4:2681. http://dx.doi.org/10.1038/ncomms3681.

[7] Zav'yalov DV, Konchenkov VI, Kryuchkov SV. May kink solution to the nonlinear Klein–Gordon equation be classified as a soliton? Tech Phys 2019;64(10):1391–4. http://dx.doi.org/10.1134/S1063784219100256.

[8] Javid A, Raza N, Osman M. Multi-solitons of thermophoretic motion equation depicting the wrinkle propagation in substrate-supported graphene sheets. Commun Theor Phys 2019;71:362–6. http://dx.doi.org/10.1088/0253-6102/71/4/362.

[9] Ablowitz M, Kruskal M, Ladik J. Solitary wave collisions. SIAM J Appl Math 1979;36(3):428–43. http://dx.doi.org/10.1137/0136033.

[10] Reinisch G, Fernandez J. Wave mechanics of sine-Gordon solitons. Phys Rev B 1982;25(12):7352–64. http://dx.doi.org/10.1103/PhysRevB.25.7352.

[11] Nakajima K, Mizusawa H, Sawada Y, Akoh H, Takada S. Experimental observation of spatiotemporal wave forms of all possible types of soliton-antisoliton interactions in josephson transmission lines. Phys Rev Lett 1990;65(13):1667–70. http://dx.doi.org/10.1103/PhysRevLett.65.1667.

[12] Ustinov AV, Doderer T, Huebener RP, Pedersen NF, Mayer B, Oboznov VA. Dynamics of sine-Gordon solitons in the annular josephson junction. Phys Rev Lett 1992;69:1815–8. http://dx.doi.org/10.1103/PhysRevLett.69.1815.

[13] Goodman R, Holmes P, Weinstein M. Interaction of sine-Gordon kinks with defects: Phase space transport in a two-mode model. Physica D 2002;161(1–2):21–44. http://dx.doi.org/10.1016/S0167-2789(01)00353-0.

[14] Lou S, Hu H-C, Tang X-Y. Interactions among periodic waves and solitary waves of the (n+l)-dimensional sine-Gordon field. Phys Rev E 2005;71(3). http://dx.doi.org/10.1103/PhysRevE.71.036604.

[15] Piette B, Zakrzewski W. Scattering of sine-Gordon kinks on potential wells. J Phys A 2007;40(22):5995–6010. http://dx.doi.org/10.1088/1751-8113/40/22/016.

[16] Adam C, Ciurla D, Oleś K, Romańczukiewicz T, Wereszczyński A. Sphalerons and resonance phenomenon in kink-antikink collisions. Phys Rev D 2021;104:105022. http://dx.doi.org/10.1103/PhysRevD.104.105022.

[17] Adam C, Manton NS, Oles K, Romanczukiewicz T, Wereszczynski A. Relativistic moduli space for kink collisions. Phys Rev D 2022;105:065012. http://dx.doi.org/10.1103/PhysRevD.105.065012.

[18] Martin-Vergara F, Rus F, Villatoro FR. Fractal structure of the soliton scattering for the graphene superlattice equation. Chaos Solitons Fractals 2021;151:111281. http://dx.doi.org/10.1016/j.chaos.2021.111281.

[19] Bishop AR. Nonlinear mode phenomenology for sine–Gordon breather excitations. J Phys A: Math Gen 1981;14(6):1417–30. http://dx.doi.org/10.1088/0305-4470/14/6/018.

[20] Kudryavtsev A, Piette B, Zakrzewski WJ. Mesons, baryons and waves in the baby Skyrmion model. Eur Phys J C 1998;1(1):333–41. http://dx.doi.org/10.1007/BF01245822.

[21] Malomed BA, Rosanov NN, Fedorov SV. Dynamics of nonlinear Schrödinger breathers in a potential trap. Phys Rev E 2018;97:052204. http://dx.doi.org/10.1103/PhysRevE.97.052204.

[22] Makhankov V. Dynamics of classical solitons (in non-integrable systems). Phys Rep 1978;35(1):1–128. http://dx.doi.org/10.1016/0370-1573(78)90074-1.

[23] Watkins R. Theory of oscillons. DART-HEP-96/03, 1996, URL: https://www.researchgate.net/publication/358445383.

[24] Cyncynates D, Giurgica-Tiron T. Structure of the oscillon: The dynamics of attractive self-interaction. Phys Rev D 2021;103:116011. http://dx.doi.org/10.1103/PhysRevD.103.116011.

[25] Taki M, Spatschek K, Fernandez J, Grauer R, Reinisch G. Breather dynamics in the nonlinear Schrödinger regime of perturbed sine-Gordon systems. Physica D 1989;40(1):65–82. http://dx.doi.org/10.1016/0167-2789(89)90027-4.

[26] Zav'yalov DV, Konchenkov VI, Kryuchkov SV. Breather solution of non-linear Klein-Gordon equation. 2022, http://dx.doi.org/10.48550/ARXIV.2204.11366.

[27] Saffin PM, Tranberg A. Oscillons and quasi-breathers in D+1 dimensions. J High Energy Phys 2007;2007(01):030. http://dx.doi.org/10.1088/1126-6708/2007/01/030.

[28] Ferreira LA, Zakrzewski WJ. Breather-like structures in modified sine–Gordon models. Nonlinearity 2016;29(5):1622–44. http://dx.doi.org/10.1088/0951-7715/29/5/1622.

[29] Martin-Vergara F, Rus F, Villatoro FR. Padé numerical schemes for the sine-Gordon equation. Appl Math Comput 2019;358:232–43. http://dx.doi.org/10.1016/j.amc.2019.04.042.

[30] Martin-Vergara F, Rus F, Villatoro FR. Padé schemes with richarson extrapolation for the sine-Gordon equation. Commun Nonlinear Sci Numer Simul 2020;85:105243. http://dx.doi.org/10.1016/j.cnsns.2020.105243.

[31] Ben-Yu G, Pascual PJ, Rodriguez MJ, Vázquez L. Numerical solution of the sine-Gordon equation. Appl Math Comput 1986;18(1):1–14. http://dx.doi.org/10.1016/0096-3003(86)90025-1.

[32] Strauss W, Vázquez L. Numerical solution of a nonlinear Klein–Gordon equation. J Comput Phys 1978;28:271–8. http://dx.doi.org/10.1016/0021-9991(78)90038-4.

[33] Buckingham R, Miller PD. Exact solutions of semiclassical non-characteristic Cauchy problems for the sine-Gordon equation. Physica D 2008;237(18):2296–341. http://dx.doi.org/10.1016/j.physd.2008.02.010.

[34] Rashid S, Kubra KT, Sultana S, Agarwal P, Osman M. An approximate analytical view of physical and biological models in the setting of Caputo operator via elzaki transform decomposition method. J Comput Appl Math 2022;413:114378. http://dx.doi.org/10.1016/j.cam.2022.114378.

[35] Rezazadeh H, Osman M, Eslami M, Ekici M, Sonmezoglu A, Asma M, Othman W, Wong B, Mirzazadeh M, Zhou Q, Biswas A, Belic M. Mitigating internet bottleneck with fractional temporal evolution of optical solitons having quadratic–cubic nonlinearity. Optik 2018;164:84–92. http://dx.doi.org/10.1016/j.ijleo.2018.03.006.

[36] García-Cervantes H, López-Becerra A, Rodríguez-González R, Rodríguez-Vargas I. Bandgap engineering in massive-massless graphene superlattices. Physica B 2022;640:414052. http://dx.doi.org/10.1016/j.physb.2022.414052.

[37] Kryuchkov S, Kukhar' E, Zav'yalov D. Charge dynamics in graphene and graphene superlattices under a high-frequency electric field: A semiclassical approach. Laser Phys 2013;23(6):065902. http://dx.doi.org/10.1088/1054-660X/23/6/065902.